TRANSIENT RESPONSE OF REVOLVING MAGNETIC FIELD IN INDUCTION TYPE BEARINGLESS MOTORS WITH SECONDARY RESISTANCE VARIATIONS

Akira Chiba,[1] Kazuhisa Yoshida,[2] Tadashi Fukao[3]

ABSTRACT

Optimal parameter selection in a field oriented control method for induction type bearingless motors is proposed to realize stable magnetic suspension. It is experimentally shown that the magnetic suspension is stable with a slight increase in a reference value of a secondary resistance. With the proper value in the secondary resistance reference, a phase angle of generated revolving magnetic field can be adjusted. There is an optimal reference value in the secondary resistance, which realizes the exact correspondence between the controller flux reference and generated revolving magnetic field. It is shown that a flux waveform, obtained from a search coil wound around a stator tooth, is corresponding to the direction of flux reference if operated with the optimal value. It is also shown that successful magnetic suspension without coupling in two orthogonal radial axes can be realized with the optimal reference value.

INTRODUCTION

In the applications of machine tools, turbo-molecular pumps, compressors, blowers, compact generators and flywheels, magnetic bearings have been used. However, conventional magnetic bearings occupy large area. Magnetic bearings require a number of wirings as well as many single phase inverters. Bearingless motors, i.e., a hybrid of electrical motors and

[1]Science University of Tokyo, Department of Electrical Engineering, Faculty of Science and Technology, 2641 Yamazaki, Noda, Chiba, Japan 278-8510.
[2]Chiba Laboratory, Science University of Tokyo, Japan 278-8510.
[3]Tokyo Institute of Technology, Department of Electrical and Electronic Engineering, Ookayama, Meguro, Tokyo, Japan 152-8552.

magnetic bearings, have been expected to reduce dimensions, a number of inverters and a cost.

Principles and basic characteristics of permanent magnet [1-3], reluctance [4-6], induction [7-11] type bearingless motors have been reported. In permanent magnet bearingless motors, design and mathematical representation have been reported in [1]. The improvements with salient pole permanent magnet motors are suggested in [2]. In the synchronous reluctance motors, controller configuration is proposed including armature reaction, and parameter variations caused by magnetic saturation [4]. Experimental results of test machines are shown in [5]. Switched reluctance type bearingless motors are also proposed [6].

In induction type bearingless motors, an experimental result was shown in [7]. It was shown that only 0.0056 times of voltage and current at motor winding terminals is required at radial force winding terminals. This result indicates possible cost down in bearingless motors. As for controller configuration, a vector control method has been proposed by Dr. Schöb for an induction type bearingless motor [8]. The radial position control for magnetic suspension seems to be successfully done in loaded conditions as a result of an extensive work. However, the proposed controller configuration is quite complicated because some flux vectors are directly controlled with outputs of some observers. It is important to have a simple controller and apply an indirect field oriented control method to eliminate flux sensors and improve reliability.

An indirect field oriented control method of induction type bearingless motors has been proposed by the authors [11]. Successful operations in loaded conditions as well as transient conditions have been shown. It has been experimentally learned that the magnetic suspension becomes stable with a slight increase in a reference value of a secondary resistance. However, the reason of the improvements in radial position control loop has not been reported.

In this paper, it is shown that the increase in the reference value in the secondary resistance results in improved characteristics in magnetic suspension. With an increase in the reference value in the secondary resistance, it is shown that a phase angle of generated revolving magnetic field can be adjusted. Thus, it is possible to adjust the reference to realize the exact correspondence between flux reference and generated revolving magnetic field. It is also shown that a flux waveform, obtained from a search coil wound around a stator tooth, is corresponding to the direction of flux reference if operated with the optimal reference value of the secondary resistance. Successful magnetic suspension without coupling in two orthogonal radial axes is shown with the optimal reference value.

ACCELERATION TESTS

Fig.1 shows the result of an acceleration test. The speed command $2\omega^*$ is increased as a step function, then, the shaft speed 2ω is increased as a ramp function with a full torque as a torque current command is limited to a rated value. The radial positions α and β of the shaft have significant fluctuations. The shaft is not successfully suspended as the clearance of touch down bearings is 100μ m. The Ψ_t is the detected flux waveform through an integrator connected to the terminals of a search coil wound around a stator tooth. The Ψ_c is the waveform of a flux reference value generated in an indirect field oriented controller. The flux waveforms Ψ_t and Ψ_c are not in phase. The Ψ_t has a phase lead angle with respect to the

[1]Osaka Prefecture University, Sakai, Osaka 599, Japan.

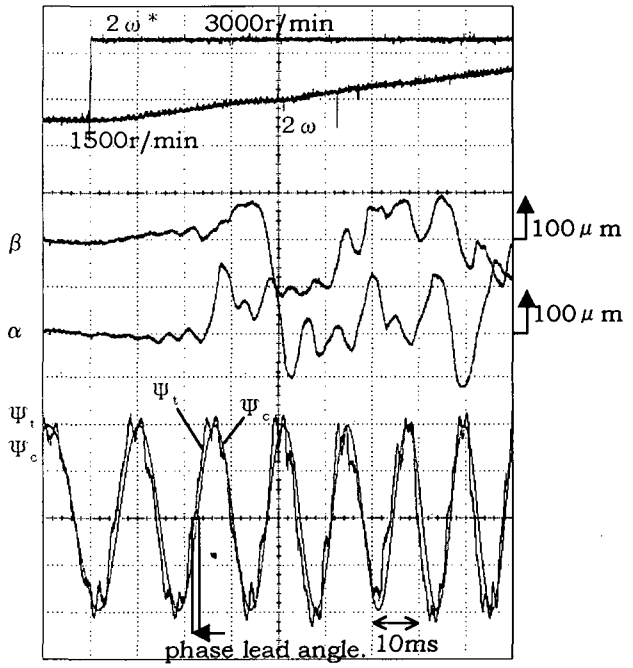

Fig.1 Acceleration test ($R_2*=R_{2L}$).

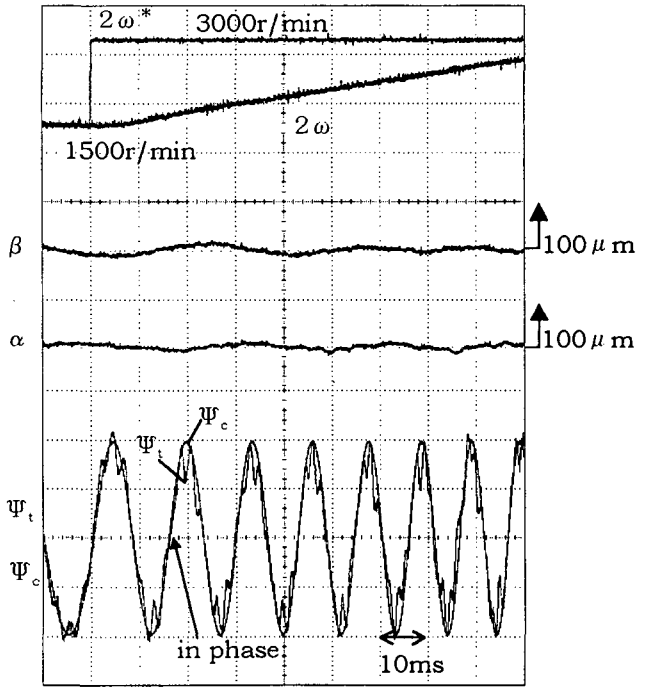

Fig.2 Acceleration test ($R_2*=R_{2o}$).

Ψ_c. The reference value R_2^* of a secondary resistance is set to the value R_{2L} obtained from a load test.

Fig. 2 shows the results of an acceleration test while the reference value R_2^* of the secondary resistance is set to R_{2O}, i.e., 1.28 times of R_{2L}. It is seen that the radial displacements are almost zero, thus, shaft touch down is avoided. The rotating shaft is successfully suspended with magnetic force during acceleration. The purpose of this paper is to find reasons why successful acceleration is realized with a slight increase in the R_2^*.

A MEASUREMENT OF SECONDARY RESISTANCE

It is important to confirm that the reference value of the secondary resistance is corresponding to the results of load tests. Figs.3 and 4 show the measured input power and line current, respectively, as a function of rotor slip while the motor windings are connected to commercial lines having a frequency of 50Hz. The line voltage is adjusted to be a constant value throughout load tests. The calculated curves from an equivalent circuit with machine parameters of $R_2^*=R_{2L}$ and $R_2^*=1.28R_{2L}$ are drawn. It can be seen that the solid curve with $R_2^*=R_{2L}$ represents the input characteristics of the induction motor. These results confirm that the R_{2L} is the exact value to realize vector control of induction motors.

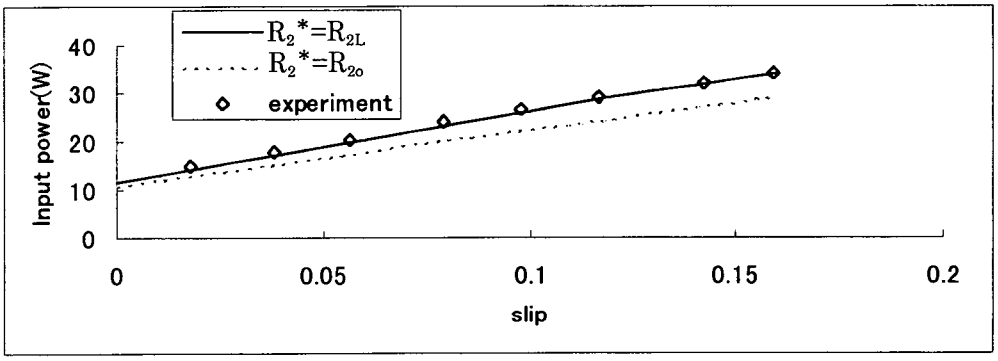

Fig.3 Input power.

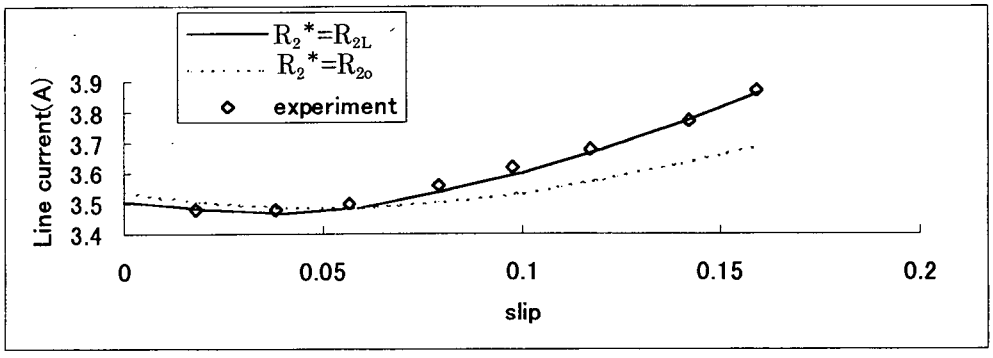

Fig.4 Line current.

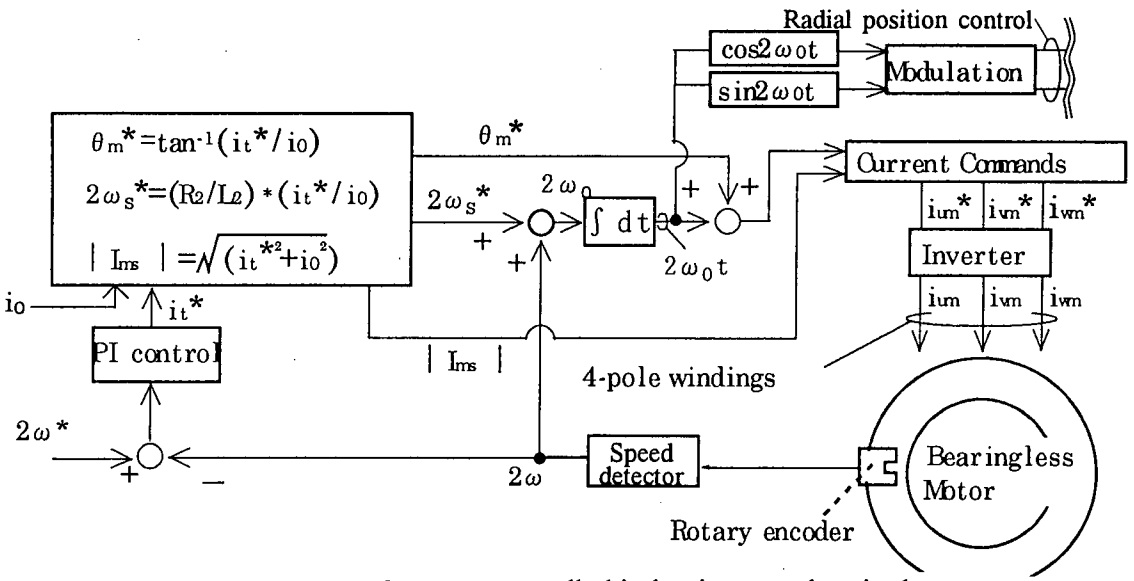

Fig.5 A block diagram of vector controlled induction type bearingless motors.

MOTOR CONTROL SYSTEM

Fig.5 shows a block diagram of the field oriented control system configuration. The shaft speed is detected and speed errors are calculated. The error is amplified in a Proportional-Integral controller. A torque current command i_t^* is generated. A flux current component i_0 is given as a constant. The amplitude of line current $|I_{ms}|$ is calculated. The phase lead angle θ_m^* is calculated from i_t^* and i_0. A slip frequency command $2\omega_s^*$ is also generated. Note that the slip frequency command is proportional to the rotor time constant. If a reference value R_2^* of a secondary resistance is the exactly the same as the actual secondary resistance, then, rotor flux linkage is kept in a constant amplitude. A smooth rotation in rotor flux linkage can be realized. The sum of $2\omega_s^*$ and detected rotor rotational speed 2ω is $2\omega_0$, which is the speed of the rotor flux linkage. The modulation components $\cos 2\omega_0 t$ and $\sin 2\omega_0 t$ are generated and used in a modulation block in a radial position controller. The three-phase current commands i_{um}^*, i_{vm}^* and i_{wm}^* are generated as,

$$i_{um}^* = |I_{ms}| \cos\left(2\omega t + \theta_m^*\right) \tag{1}$$

$$i_{vm}^* = |I_{ms}| \cos\left(2\omega t + \theta_m^* + 120^\circ\right) \tag{2}$$

$$i_{wm}^* = |I_{ms}| \cos\left(2\omega t + \theta_m^* + 240^\circ\right). \tag{3}$$

If the reference value of the secondary resistance is exactly the same as the real secondary resistance value, and if the motor winding currents are controlled to follow these references, then, the instantaneous rotor flux linkages in two perpendicular axes should be exactly the same as the controller signals of $\cos 2\omega_0 t$ and $\sin 2\omega_0 t$. Thus, the signal $\cos 2\omega_0 t$ is hereafter referred as controller flux reference Ψ_c. It is not possible to detect the rotor flux linkage, thus, it is very difficult to confirm that the direction and amplitude of the rotor flux

linkage is corresponding to the reference Ψ_c.

It is possible to have search coils around stator teeth to see flux distribution. The tooth flux density is not equal to the rotor winding flux linkage nor stator winding flux linkage. It is close to the air-gap flux linkage, however, it is not exactly the same. The obtained flux variations in a search coil provide information of the 4-pole revolving magnetic field.

Fig.6 shows the waveforms of the tooth flux linkage Ψ_t and the controller flux reference Ψ_c. The reference value of the secondary resistance is set to R_{2L}. It is seen that there is a phase lead angle in the search coil flux with respect to the flux reference in control circuits. This fact is understandable because the rotor flux linkage includes the leakage flux in addition to the air-gap flux. Physically, the detected flux in the search coil indicates flux variations which is close to the air-gap flux. Thus, it is very natural that there is a difference in phase angle.

One of the interesting point is that the phase angle is depending on the reference value R_2^* of the secondary resistance. The phase angle is also depending on load conditions. Fig.7 shows the measured phase angle variations at three operating points. One is no load condition. The others are at about a half of the rated points as a motor and a generator. The phase angle is measured at these three operating points at various reference values of the secondary resistance. If the reference value is set to a small value, the phase angle of Ψ_t is advanced with respect to Ψ_c in motor operation, however, it delayed in generator operation. On the contrary, if the reference value is high, it is delayed in motor operation but it is advanced in generator operation. It is seen that the phase angle variations can be adjusted by a proper setting in the reference value of the secondary resistance. Note that the there is no phase angle variations if the reference value of the secondary resistance is set to a particular value. This

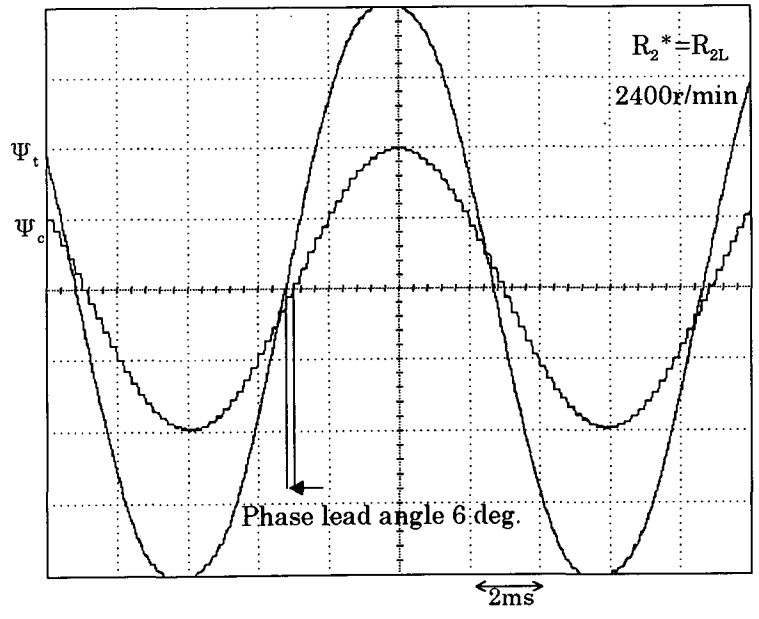

Fig.6 Waveforms of Ψt and Ψc with $R_2^*=R_{2L}$.

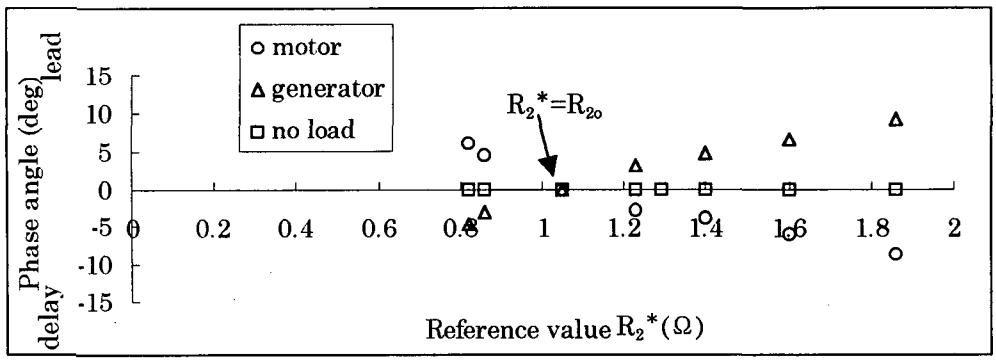

Fig.7 Phase lead angle of Ψ_t.

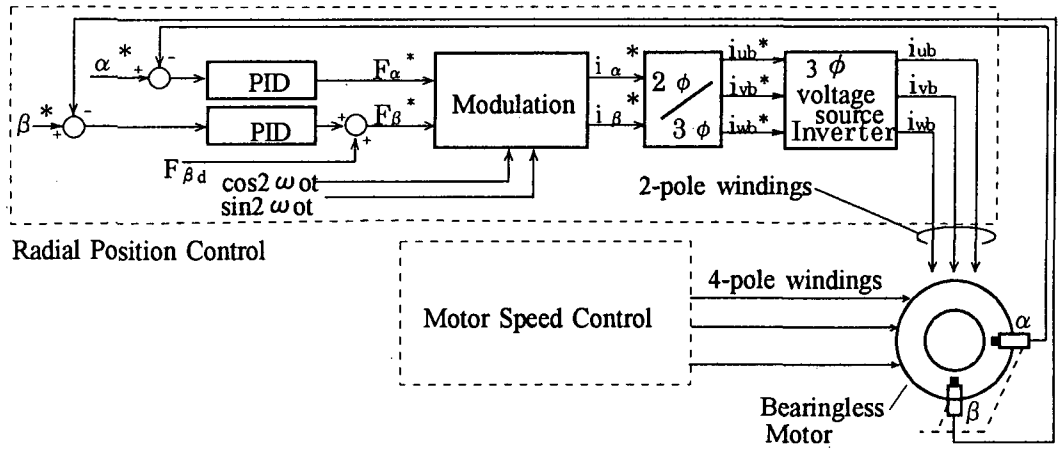

Fig.8 Radial position controller configuration.

value is hereafter referred as R_{2O}.

RADIAL POSITION CONTROL SYSTEM

Fig.8 shows a block diagram of the radial position control system. In a radial position controller, the rotor radial displacements α and β are detected by eddy current type displacement sensors. The errors are amplified in the Proportional-Integral-Differential controllers. The radial force commands F_α* and F_β* are generated. From these radial force commands, the current commands i_α* and i_β* of the 2-pole radial force windings are generated in a modulation circuit by cos2ω*t and sin2ω*t functions, as follows ;

$$\begin{pmatrix} i_\alpha^* \\ i_\beta^* \end{pmatrix} = \frac{1}{M' i_0} \begin{pmatrix} -\cos 2\omega^* t & \sin 2\omega^* t \\ \sin 2\omega^* t & \cos 2\omega^* t \end{pmatrix} \begin{pmatrix} F_\alpha^* \\ F_\beta^* \end{pmatrix} \tag{4}$$

where, M' is a derivative of mutual inductance with respect to radial position. The modulation

matrix is originated from the following matrix calculation, where ϕ denotes ω*t.

$$\begin{bmatrix} -\cos 2\phi & \sin 2\phi \\ \sin 2\phi & \cos 2\phi \end{bmatrix} = \begin{bmatrix} \cos\phi & \sin\phi \\ -\sin\phi & \cos\phi \end{bmatrix} \begin{bmatrix} -1 & 0 \\ 0 & 1 \end{bmatrix} \begin{bmatrix} \cos\phi & -\sin\phi \\ \sin\phi & \cos\phi \end{bmatrix} \quad (5)$$

The modulation matrix is a product of rotational coordinate transformation matrix, a sign matrix and an inverse matrix of the rotational coordinate transformation matrix. In this modulation, it is supposed that the sine and cosine functions indicate an exact direction of revolving magnetic field. If there is an error in the phase angle, the direction of resulted radial force is not the same as the reference, which may result in coupling in radial forces in two orthogonal axes.

The inverter is controlled by 3-phase current commands i_{ub}*, i_{vb}* and i_{wb}* and supplies the currents i_{ub}, i_{vb} and i_{wb} in the radial force windings. The variables of motor windings and radial force windings are indicated by the subscripts m and b, respectively.

Figs.9 (a) and (b) show principles of interference between α and β axes when the direction of the revolving magnetic field has phase lead angle of θ. Fig.9(a) shows radial force generation without interference. The N_4 windings indicate the equivalent current direction of revolving magnetic field. The fluxes Ψ_4 indicate the direction of 4-pole flux distribution. The equivalent windings N_β indicate the current direction of 2-pole radial force windings. The fluxes Ψ_β show the direction of 2-pole fluxes at the air-gap. In the air-gap 1, the direction of Ψ_4 and Ψ_β are the same. On the contrary, the direction of Ψ_4 and Ψ_β are opposite in the air-gap 3. Thus, radial force is generated in the β-axis direction.

Let suppose that the exciting current is advanced by an angle of 2θ. Then, the 4-pole revolving magnetic field is advanced by a mechanical angle of θ with respect to the flux reference in controllers. In Fig.9(a), N'_4 windings shows the positions of equivalent windings of 4-pole magnetic field with the advanced angle of θ. The equivalent windings are written in dotted lines. In Fig.9(b), α'- and β'-axes are drawn corresponding to the rotation of revolving magnetic field. Let examine a case when a current exists only in N_β winding. The equivalent current in N_β winding can be represented by N'_α and N'_β current components in the α'- and β'-axes. With the current in N'_β, the flux Ψ'_β is generated. With an interaction of 4-pole fluxes Ψ'_4, a radial force of F_β' is generated. With the current in N'_α, the 2-pole flux Ψ'_α is generated, which results in a radial force of F_α' with an interaction of 4-pole fluxes. The resulted radial force is F '. The direction of the generated radial force is advanced by an angle of 2θ. This fact indicates that the mutual interference is caused between two perpendicular α and β axes when the 4-pole flux has a phase lead angle with respect to the controller flux reference.

MEASUREMENTS OF INTERFERENCE OF RADIAL FORCES

In this section, mutual interference is experimentally measured. A static radial force is externally applied to a shaft of a test machine by a weight through a pulley. The electro magnetic radial force is generated by a bearingless motor unit to keep force balance. Radial force commands F^*_α and F^*_β are automatically generated by negative feedback loops in radial position controllers. Let us define the radial force command vector F* as the vector sum

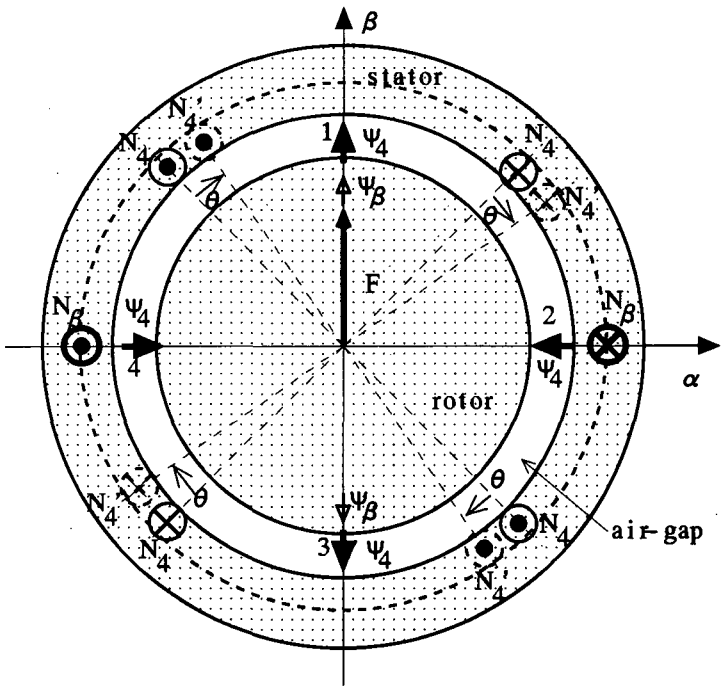

(a) Exact field flux orientation.

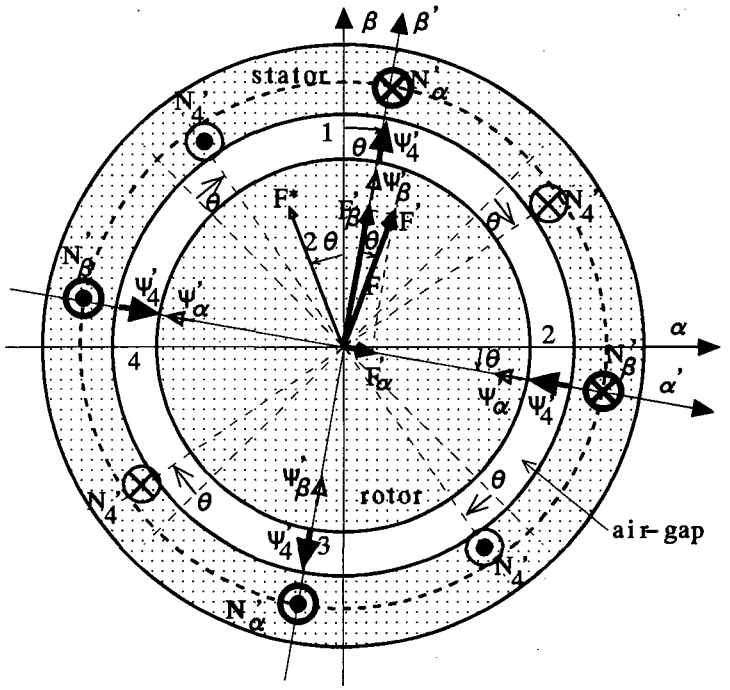

(b) The 4-pole Flux with an advanced angle of θ.

Fig.9 The variations in the radial force direction depending on the 4-pole flux orientation.

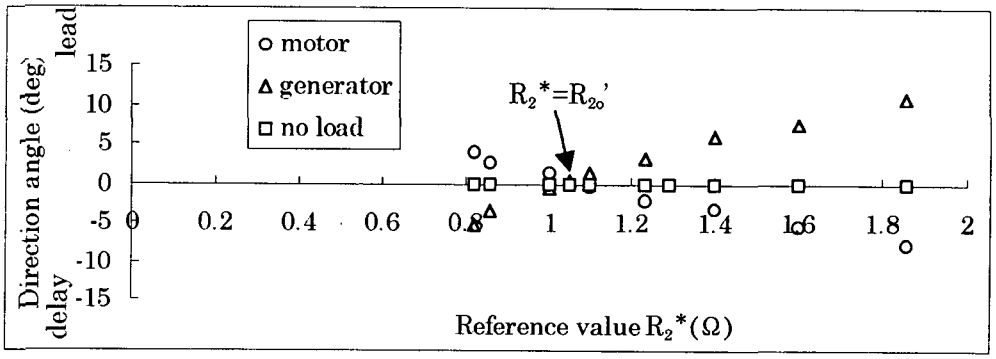

Fig.10 Direction of radial force reference in controllers.

of F^*_α and F^*_β. If the flux reference in the controller is exactly the same as the actual flux in a bearingless motor, the direction of the radial force command F* is exactly opposite to the direction of the external radial force. However, the direction of the radial force command is delayed by 2θ if the 4-pole magnetic field is advanced by θ. The direction of the radial force command F* is drawn in Fig.9(b) for this case.

Fig.10 shows the measured direction of radial force command at three different operating points, i.e., no load and motor and generator operating at a half load of the rated points. If the reference value of the secondary resistance is small, then, the phase angle of radial force command is delayed in motor operations. This process can be explained as follows;

(i) If the reference value of the secondary resistance is set to a small value, then, the 4-pole flux is advanced with respect to the flux reference in a vector controller as previously shown in Figs.6 and 7.

(ii) The advanced 4-pole revolving magnetic field results in advanced radial force generation in bearingless motors.

(iii) To keep the force balance to realize successful shaft suspension, the negative feedback loops automatically adjust radial force command to have a phase delay.

(iv) Thus, the resulted radial force command is delayed.

On the contrary, in generator operations, the 4-pole revolving magnetic field is delayed. The radial force command having a phase lead angle is automatically generated. This fact verifies that there is mutual interference in radial force generation in α and β axes. The interference of the radial force is depending on the load conditions. However, there is a particular reference value in secondary resistance. It is noted that the direction angle is zero in both motor and generator operations when the reference value of the secondary resistance is equal to R'_{2O}. This result indicates that there is an optimal value in the secondary resistance reference, which realizes no mutual interference in two perpendicular axes.

Fig.11 and Fig.12 shows waveforms of step disturbance suppression. External disturbance electrical signal is added in β radial position control loop as shown in Fig.8. Fig.11 shows the waveforms operating at $R_2^*=R_{2L}$. Fig.12 shows the waveforms with a

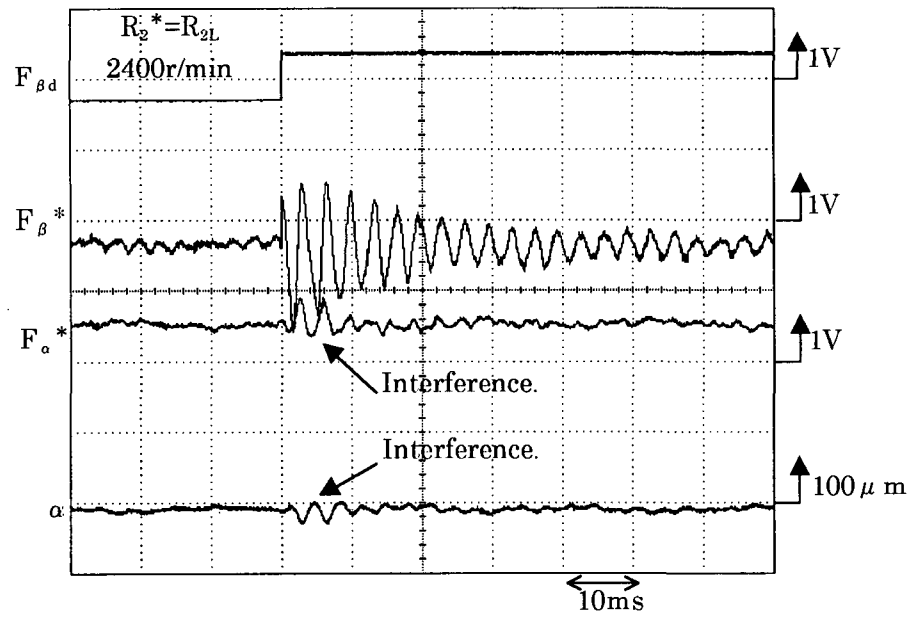

Fig.11 Step disturbance suppresion under load with $R_2^*=R_{2L}$.

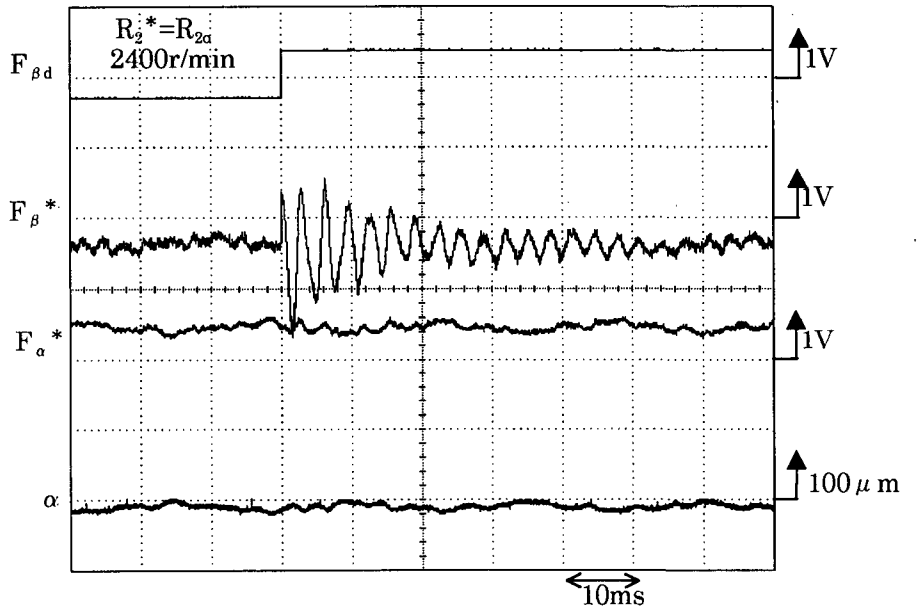

Fig.12 Step disturbance suppresion under load with $R_2^*=R_{2o}$.

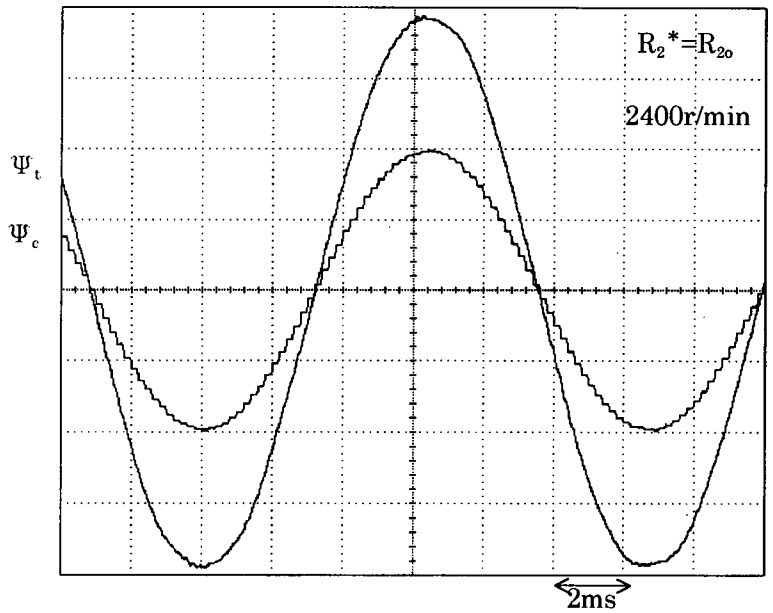

Fig.13 Waveforms of Ψt and Ψc with R_2*=R_{2o}.

controller having the optimal reference value of the secondary resistance, i.e., R_2*=R'_{2O}. It is seen that the step disturbance in the β-axis has influence in the α-axis in Fig.12. However, the interference is less in Fig.13.

It is also interesting that the value of R'_{2O} is almost the same as the reference value R_{2O}, which realizes close correspondence between the controller flux reference and search coil flux as previously shown in Fig.7. The discrepancy is within the error of the measurements. Fig.13 shows the waveforms of Ψ_c and Ψ_t at R_2*=R'_{2O}. It is seen that the two waveforms are almost in phase.

ACCELERATION TEST IN SIMULATION

In the preceding chapters, the optimal reference value of the secondary resistance is found. With the optimal reference, it is also shown that the controller flux reference is corresponding to the search coil flux. These results are obtained from experiments in steady state conditions. It is important to see transient response.

Figs.14 and 15 shows the results of computer simulations. In the simulation, an induction motor is represented by instantaneous values having constraints of vector control theory. The speed command is increased as a step command as in the case of Figs.1 and 2. In addition, amplitudes and phase lead angles of the secondary flux linkage and air-gap flux linkage with respect to the controller flux reference are also shown. In Fig.14, the reference value R_2* of the secondary resistance is set to R_{2L}. The amplitude and phase of the secondary

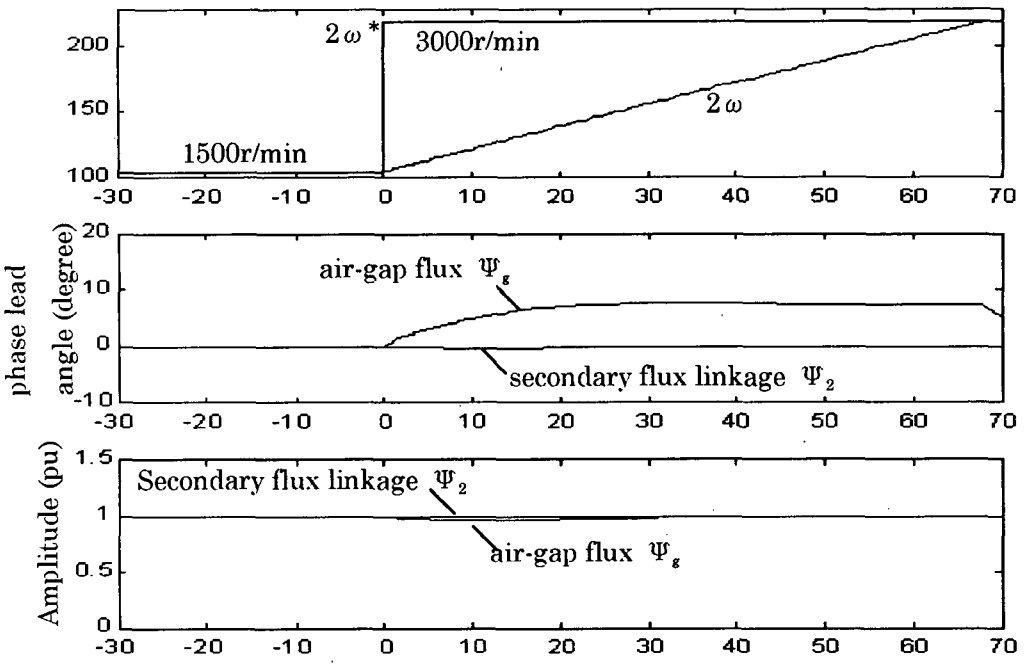

Fig.14 Calculated waveforms at $R_2^*=R_{2L}$ in simulation.

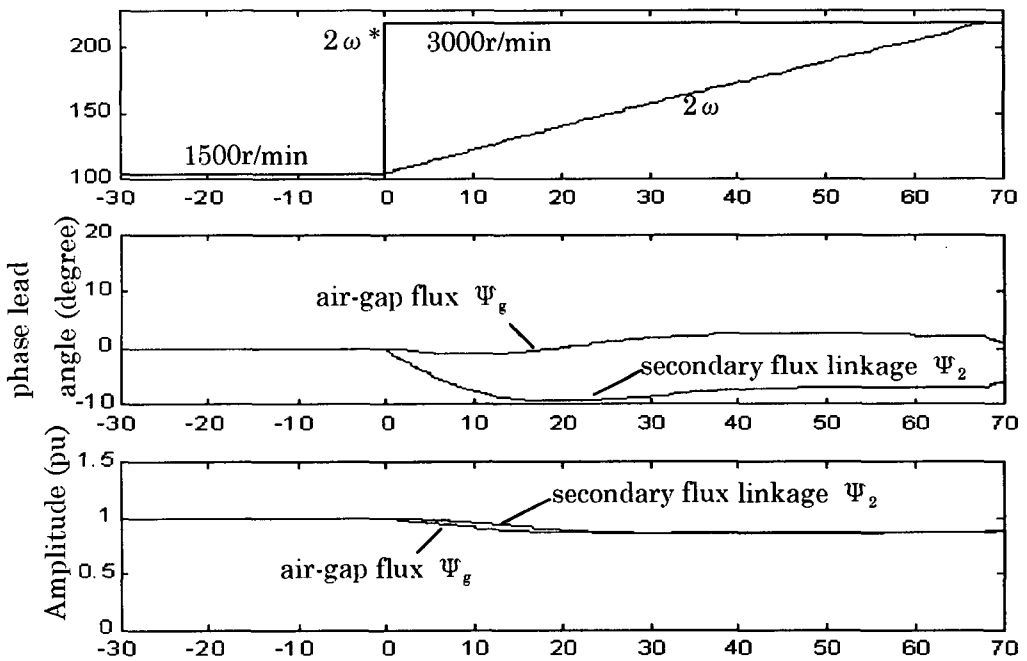

Fig.15 Calculated waveforms at $R_2^*=R_{2o}$ in simulation.

flux linkage is exactly the same as the controller flux reference. In Fig.15, the reference value R_2* of the secondary resistance is set to R_{2O}. The rotor flux linkage has variations, however, the air-gap flux is almost constant. The result indicates that the air-gap flux and controller flux reference are in phase at R_2*=R_{2O}. In this setting, the experimental results shown in Fig.2 indicate the successful acceleration.

CONCLUSION

Parameter selections of a field oriented control of induction type bearingless motors with a slip frequency control is reported for stable radial position control loops. The main conclusions can be summarized as follows;

(i) With optimal reference value R_{2O} in the secondary resistance, the decoupling of radial force is found to be realized.

(ii) It is experimentally shown that the controller flux reference is corresponding to search coil flux linkage at the optimal reference value. It is theoretically shown that the air-gap flux linkage is corresponding to the controller flux reference.

(iii) It is shown that stable acceleration can be realized with the optimal reference. During the acceleration, the direction of the air-gap flux is corresponding to the flux reference.

REFERENCES

[1] Masahide Ooshima, Satoru Miyazawa, Akira Chiba, Fukuzo Nakamura and Tadashi Fukao, "A Rotor Design of a Permanent Magnet-Type Bearingless Motor Considering Demagnetization", IEEE Proceeding of Power Conversion Conference (PCC-Nagaoka) pp.655-660 Nagaoka, August 6, 1997

[2]Y. Okada, K. Dejima, T. Oshima,"Analysis and Comparison of PM Synchronous Motor and Induction Motor Type Magnetic Bearings", IEEE Trans. IA-31, no.5 pp.1047-1053, 1995

[3] T.Le Magueresse and G.Lemarquand "A Comparative Analysis of Permanent Magnet-type Synchronous Motors for Fully Magnetically Levitated Rotors", MMM-Intermag EQ12 San Francisco 1998

[4] Chikara Michioka, Tomokazu Sakamoto, Osamu Ichikawa, Akira Chiba and Tadashi Fukao, "A Decoupling Control Method of Reluctance-Type Bearingless Motors Considering Magnetic Saturation", IEEE Transaction on Industry Applications, vol.32, no.5, pp.1204-1210, Sept/Oct., 1996

[5] S.Mori, T.Satoh and M.Ohsawa, "Experiments on a Bearingless Synchronous Reluctance Motor with Load", Fifth International Symposium on Magnetic Bearings, Kanazawa, 1996, pp.339-343

[6] Masatsugu Takemoto, Ken Shimada, Akira Chiba and Tadashi Fukao,"A Design and Characteristics of Switched Reluctance Type Bearingless Motors", 4th International Symposium on Magnetic Suspension Technology, Gifu, Oct.30

[7] Eichi Ito, Akira Chiba and Tadashi Fukao," A Measurement of VA Requirement in a Induction Type Bearingless Motor",4th International Symposium on Magnetic Suspension Technology, Gifu, Oct.30

[8] R. Schob, J. Bichsel, "Vector Control of the Bearingless Motor", Fourth International Symposium on Magnetic Bearing, Zurich 1994

[9] J.A.Santisteban, A.O.Salazar, R.M.Stephan and W.G.Dunford, "A Bearingless Machine -

An Alternative Approach", Fifth International Symposium on Magnetic Bearings, Kanazawa, 1996, pp.345-349
[10] Y. Takamoto, A. Chiba, T. Fukao, "Test Results on a Prototype Bearingless Induction Motor with Five-Axis Magnetic Suspension", IPEC-Yokohama '95, April pp.334-339, 1995
[11] Akira Chiba, Ryusaku Furuichi, Yoshiteru Aikawa, Ken Shimada, Yasuhisa Takamoto and Tadashi Fukao, "Stable Operation of Induction-Type Bearingless Motors Under Loaded Conditions", IEEE Transaction on Industry Applications, vol.33, no.4, pp.919-924, July/August, 1997